

Supporting Information

Wearing “Body Armor” on Zinc anodes for Robust Aqueous Zinc-ion Batteries

Qunhao Wang,^{a,1} Xueyong Deng,^{a,1} Xiaolin Xue,^a Jian Zhang,^b Jiangqi Zhao,^c Zengyan Sui,^a Yuefei Zou,^a Longbo Luo,^a Wei Zhang,^{a,d,} Xiangyang Liu,^{a,*} Canhui Lu,^{a,d}*

a. State Key Laboratory of Polymer Materials Engineering, Polymer Research Institute, College of Polymer Science and Engineering, Sichuan University, Chengdu 610065, China.

b. Fujian Provincial Key Laboratory of Environmental Engineering, Fujian Provincial Academy of Environmental Science, Fujian, 350013, China

c. College of Materials Science and Engineering, Sichuan University, Chengdu 610065, China

d. Advanced Polymer Materials Research Center of Sichuan University, Shishi 362700, China.

*Authors for correspondence: weizhang@scu.edu.cn (W. Z.), lxy@scu.edu.cn (X. L.)

¹ These authors contributed equally to this work.

Table of contents

Supplementary Experiments

Supplementary Figures 1 to 21

Supplementary Video Captions 1 to 2

Experimental Section

Materials

Commercial carbon cloth (CC, W0S1009) was received from CeTech Co., Ltd., Beijing, China. Sodium bromide (NaBr), sodium hypochlorite (NaClO), sodium hydroxide (NaOH), sulfuric acid (H₂SO₄), and hydrochloric acid (HCl) were provided by Kelong Reagent Co., Ltd., Chengdu, China. 2,2,6,6-Tetramethyl-piperidin-1-oxyl (TEMPO) was purchased from Aladdin Reagent Co., Ltd., Shanghai, China. Activated carbon and Poly(tetrafluoroethylene) (PVDF) were provided by Kluthe Chemical Technology Co., Ltd., Shanghai, China. Zinc sulfate heptahydrate (ZnSO₄·7H₂O) and N-methylpyrrolidone (NMP) were purchased from Sinopharm Group Chemical Reagent Co., Ltd., Shanghai, China. Manganese sulfate (MnSO₄) was purchased from Macklin Biochemical Technology Co., Ltd., Shanghai, China. No further treatment was conducted on these chemicals before use.

Materials preparation

Preparation of ANF suspension: To prepare the ANF dispersion, 100 ml of DMSO was added to a 250 ml flask, followed by the addition of deionized H₂O (4 ml), KOH (1.5 g) and Kevlar fibers (1 g). The mixture was then mechanically stirred at 400 rpm for 3 days in the absence of moisture and light. The resulting dark red dispersion was centrifuged twice at 8000 rpm, 25°C for 10 min to remove impurities. The dispersion was stored at 25°C, sealed and protected from moisture and light. The concentration of ANF was measured after each preparation batch. To determine the concentration, a certain amount of the dispersion was soaked in water to replace the solvent and then dried to obtain the solid content.

Preparation of CNF suspension: First, 30 g of cellulose pulp plates was added in 3000 mL distilled water and stirred for 8 h at room temperature. Then, 1.543 g NaBr and 0.234 g TEMPO were added and stirred at room temperature. After NaBr and TEMPO were completely dissolved, 96.8 g of 11 wt.% NaClO solution was added. During the subsequent reaction, the pH of the system

was adjusted to 10 by adding 0.1 M HCl and 0.2 M NaOH, under continuous stirring at room temperature. When the pH of the system did not change, the reaction was terminated. Subsequently, the obtained mixture was added to 3000 mL of water and wet-milled using an ultra-fine friction grinder Supermass collider (MKCA6-2, Masuko Sangyo Co., Ltd., Japan) at 1500 rpm (with a clearance between two grinding disks of $-100\ \mu\text{m}$). Following 10 cycles of wet-milling, a homogeneous CNF aqueous dispersion was obtained.

Preparation of ANF/CNF membrane: AC membranes were prepared by vacuum-assisted filtration. A given amount of ANF dispersion was first diluted to $0.2\ \text{mg mL}^{-1}$ by adding DMSO with stirring for 30 min, then 8 mL of CNF dispersion ($2\ \text{mg mL}^{-1}$) was added to 80 mL of ANF dispersion. The dispersions were stirred vigorously for 2 h. The homogeneous mixture was treated by vacuum filtration using PTFE filter membranes with a pore size of $0.1\ \mu\text{m}$. Finally, the assembled networks were washed with DI water and peeled off the membranes with tweezers.

Preparation of MnO₂: The MnO₂ powders were first synthesized by a facile hydrothermal method as follows: 0.456 g MnSO₄ and 0.1 g H₂SO₄ (98 wt.%) were added to 90 mL deionized water at room temperature with magnetic stirring for a clear solution. Then, 20 mL 0.1 M KMnO₄ aqueous solution was slowly added into the above solution. The mixture was stirred for 2 h. Next, the solution was transferred into a Teflon-lined autoclave and heated at 120°C for 12 h. After naturally cooled down to the room temperature, the MnO₂ was washed 3 times with distilled water and dried at 60°C for 6 h.

Preparation of MnO₂@CC cathode: To prepare the MnO₂@CC cathode, the MnO₂ powders, carbon black, and PVDF were blended in a weight ratio of 7:2:1 in the NMP solvent. The resultant slurry was then coated on circular carbon cloth with a diameter of 8 mm or a rectangular carbon cloth with dimensions of 20 mm \times 15 mm. After drying at 80°C for 6 h to remove residual solvent, the MnO₂@CC cathode was obtained. The MnO₂ loadings of the circular MnO₂@CC cathodes were uniformly about $1.5\ \text{mg cm}^{-2}$ unless otherwise specified. The MnO₂ loadings of the

rectangular MnO₂@CC cathodes of the pouch cells in Fig. 5h and 5i are 1 and 5 mg cm⁻², respectively.

Materials Characterization

Surface topography and interfacial failure topography of the composite membrane were observed by a Field-Emission Scanning Electron Microscopy (FESEM) on Regulus8220 (Hitachi, Japan), and all samples were sputtered with Au to form a conductive layer and collect electronic signals. The chemical structures of the samples were measured by using an FTIR spectroscope (Perkin Elmer) at room temperature in the 4000–500 cm⁻¹ range with a resolution of 4 cm⁻¹. The crystal structures were characterized by XRD (Rigaku Ultima IV) equipped with Cu Ka irradiation from 5° to 85°. The mechanical properties of membranes were measured using a KOL KD III-5000 mechanical tester with a sample rectangle size of 20 × 5 mm² and a loading rate of 0.5 mm min⁻¹ at room temperature, and each sample was measured for 5 times. Water contact angle tests were performed on a contact angle tester (DSA-25).

Electrochemical measurement

The electrochemical tests were conducted on CR 2032 coin-type cells with 2 M ZnSO₄ electrolytes, unless otherwise specified. The Zn plating/stripping process was investigated in an asymmetric cell system using a Cu foil (thickness of 50 μm, diameter of 8 mm) as cathode, a Zn foil as anode. For the symmetric cell system, two identical Zn foils were assembled. Note that, the assembly of AC-based Zn symmetric batteries necessitates the utilization of two AC interlayers, which are positioned between the separator and the Zn electrodes on each side. As for full batteries, the MnO₂@CC (diameter of 8 mm) and Zn foil were applied as the cathode and anode, respectively. Unless otherwise specified, the Zn foil utilized in the experiments has a thickness of 50 μm and a diameter of 8 mm. The full battery performance was studied at different current densities within 1.0–1.8 V voltage window. Cyclic voltammograms (CV), Tafel tests, chronoamperometry (CA) curves, and electrochemical impedance spectra (EIS) were tested on a

CHI 760E electrochemical workstation (Shanghai ChenHua Instruments, China). A Land 2001A battery testing system (Wuhan LAND electronics, China) was used to measure the galvanostatic charge/discharge (GCD) curves and cycling performance of the batteries.

Ionic conductivity measurements: The ionic conductivity (σ) values of the membranes infiltrated with the electrolyte were measured by EIS tests using stainless steel/membrane/stainless steel symmetric cells. The σ (mS cm^{-1}) can be calculated from the following equation:

$$\sigma = \frac{L}{RS}$$

where L is the thickness of the separator, S is the contact area between the membrane and the stainless steel electrode, and R (Ω) represents the bulk resistance acquired from the intercept of Nyquist plots with the real axis.

Zn²⁺ transference number measurements: The Zn²⁺ transference number ($t_{\text{Zn}^{2+}}$) was measured through CA and EIS tests on Zn//Zn symmetric cells and calculated by the following equation:

$$t_{\text{Zn}^{2+}} = \frac{I_s(\Delta V - I_0 R_0)}{I_0(\Delta V - I_s R_s)}$$

where I_0 and I_s are the initial and steady-state current, respectively, ΔV is the applied constant potential (10 mV), and R_0 and R_s are the initial and steady-state interface impedances of the cells that were determined by EIS tests, respectively.

Computational simulation

Density functional theory (DFT) calculation: The binding energies between ANF, CNF molecules or H₂O and Zn²⁺, and corresponding electrostatic potential (ESP), were respectively calculated by DMol3 module in MS 20201. Firstly, the generalized gradient approximation (GGA) with Perdew–Burke–Ernzerhof (PBE) exchange–correlation functional was employed to fully relax ANF, CNF, and H₂O molecules. The double-numeric quality basis sets with polarization functions were used. The iterative tolerances for energy change, force and displacements were

1×10^{-5} Ha, $0.002 \text{ Ha } \text{\AA}^{-1}$ and 0.005 \AA , respectively. In the self-consistent field (SCF) procedure, 10^{-6} a.u. was used for the convergence standard electron density. After structure optimization, the Adsorption Locator Tools in MS were used to locate Zn^{2+} at energy favorable site of H_2O , ANF, and CNF molecules. Then each pair was freely optimized by DMol3 module. The binding energies E_b were calculated according to the following equation:

$$E_b = E_{total} - E_{molecule} - E_{\text{Zn}^{2+}}$$

Where E_{total} is total energy of the interaction pair, $E_{molecule}$ is the energy of isolated molecule, namely H_2O , ANF, and CNF molecules, and $E_{\text{Zn}^{2+}}$ is the energy of one Zn^{2+} .

Finite element simulations: The three semi ellipses represent the protrusions on the Zn surface. According to the structural characteristics of the AC interlayer, the models were constructed as shown in Figure S24. The phase-field model was coupled with secondary/triple current density distribution to investigate the electric field distribution, Zn^{2+} ion concentration distribution with different hydrogel electrolytes.

Figures

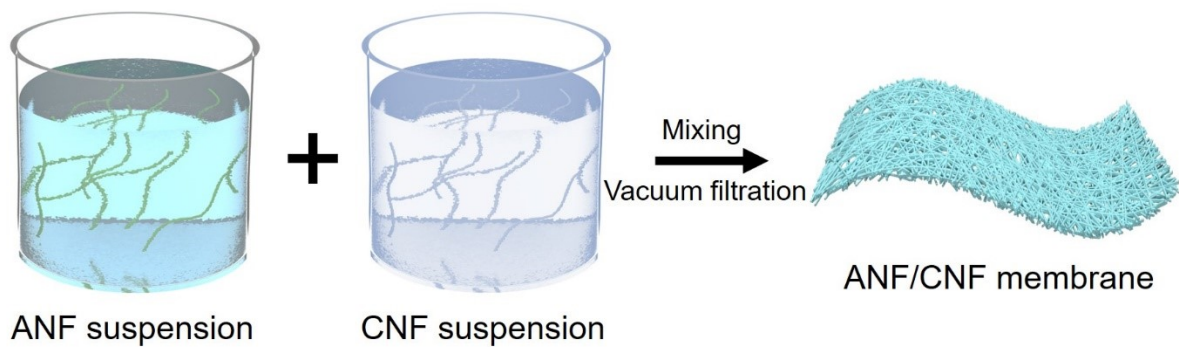


Figure S1. Schematic illustration of the preparation strategy for the ANF/CNF membrane.

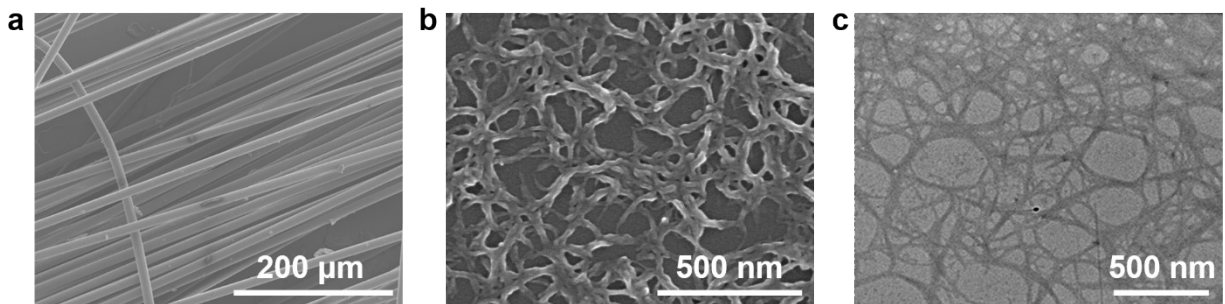


Figure S2. SEM images of (a) the Kevlar fibers and (b) ANFs. (c) TEM image of ANFs.

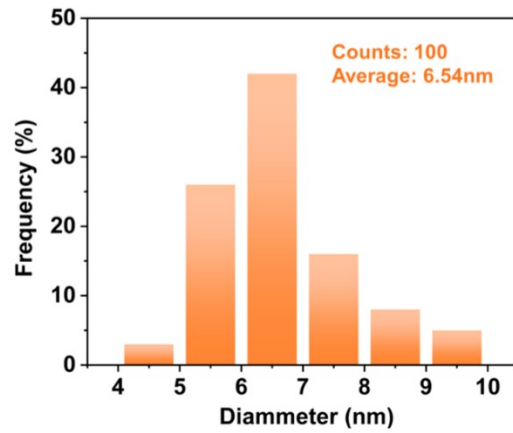


Figure S3. Diameter distribution of ANFs



Figure S4. Digital photograph of the ANF suspension.

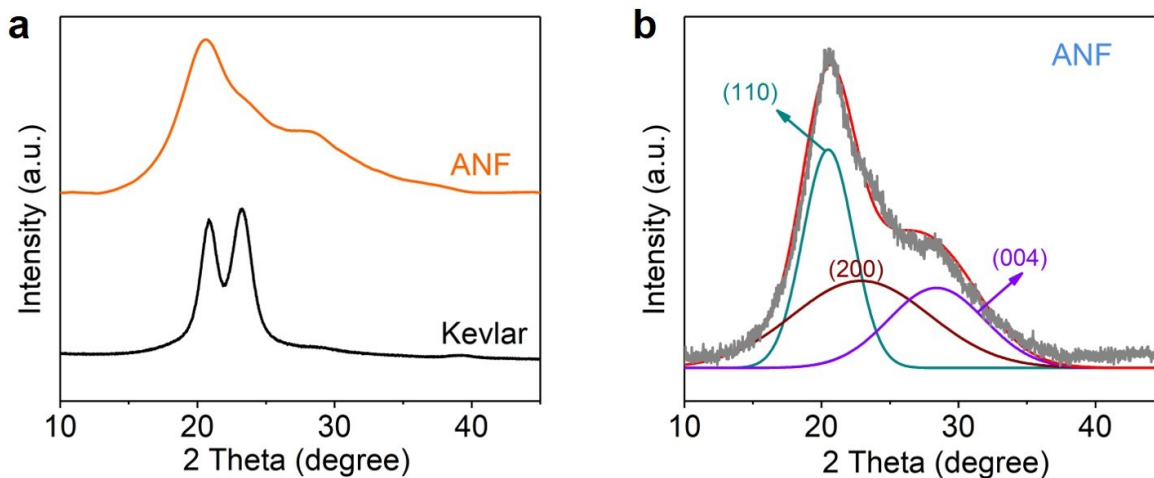


Figure S5. XRD patterns for both the pristine Kevlar fiber and the prepared ANF.

The X-ray diffraction (XRD) patterns for both the pristine Kevlar fiber and the prepared ANF are depicted in Figure S5. The three diffraction peaks at 2θ values of 20.6° , 22.9° , and 28.4° correspond to the (110), (200), and (004) planes of the poly-(paraphenylene terephthalamide), respectively. In comparison to the Kevlar fiber, the ANF exhibits significantly broadened diffraction signals, which can be attributed to the decrease in crystallinity that occurs during the deprotonation cleavage process.

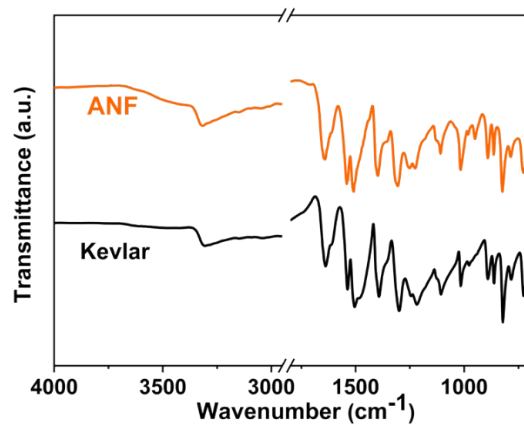


Figure S6. FTIR spectra for Kevlar fiber and the prepared ANF.

Figure S6 displays the FTIR spectra for Kevlar fiber and the prepared ANF. The absorption peaks at 1647, 1543, and 1515 cm^{-1} correspond to the stretching vibration of C=O groups, coupled N-H deformation and C-N stretching vibration signal, and the stretching vibration of C=C in aromatic rings, respectively. The characteristic peaks of the ANF are in exact alignment with those of the Kevlar fiber, thereby confirming that the ANF obtained through chemical cleavage maintains the structural integrity of the PPTA molecules.

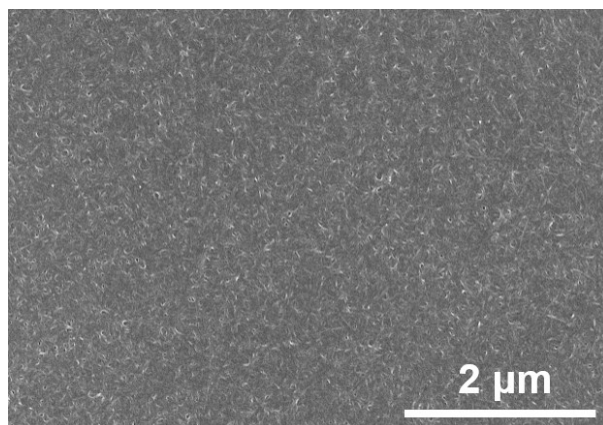


Figure S7. Surface SEM image of the AC membrane.

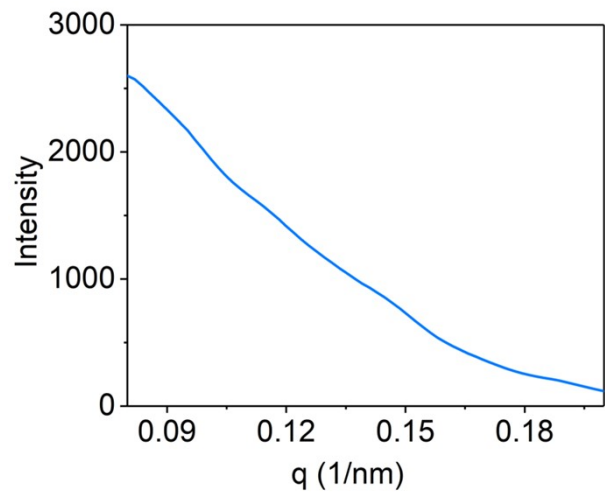


Figure S8. The SAXS I-Q curve diagram of AC membrane.

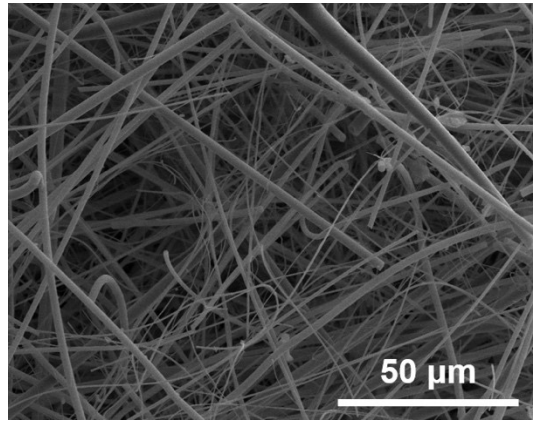


Figure S9. SEM image of the GF separator.

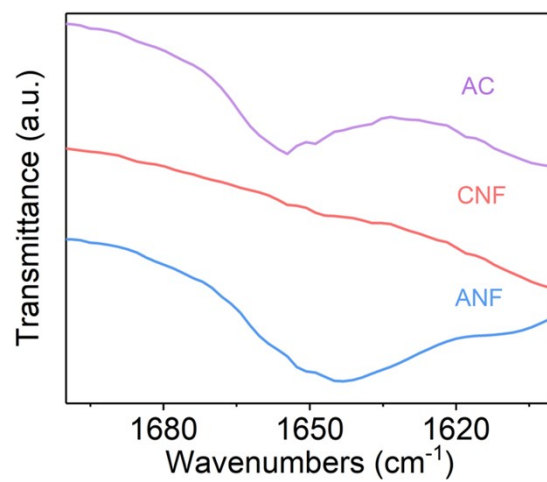


Figure S10. FTIR spectra of the ANF, CNF, and AC membranes.

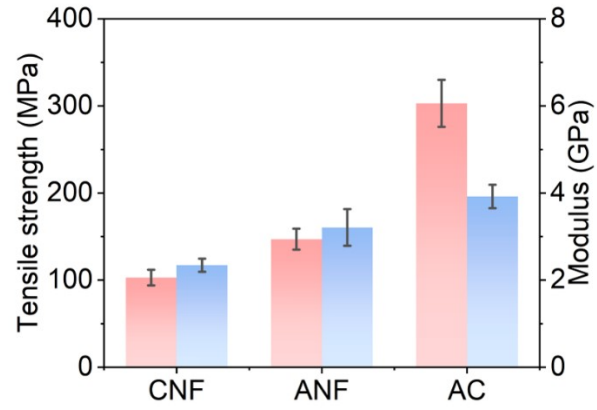


Figure S11. Tensile strength and modulus of the CNF, ANF, and AC membranes.

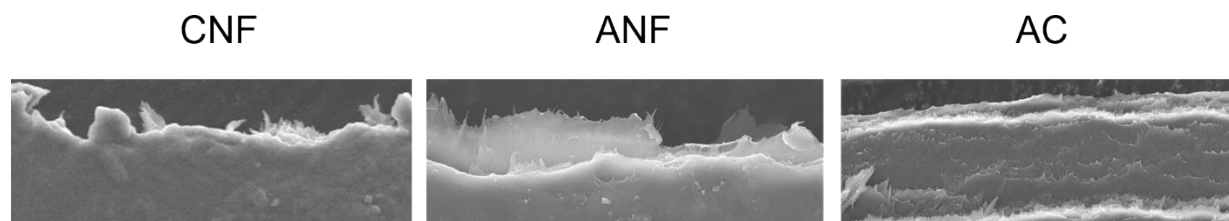


Figure S12. Cross-sectional SEM images of the tensile fracture of the CNF, ANF, and AC membranes.

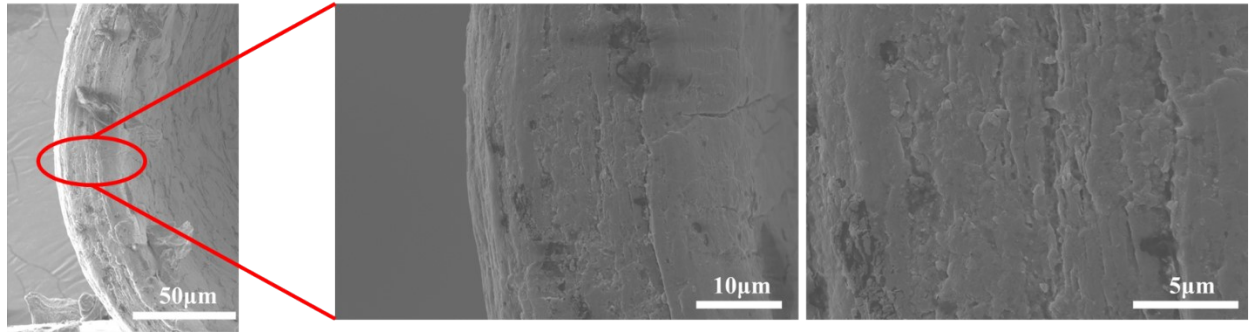


Figure S13. Cross-sectional SEM image of the folded AC membrane

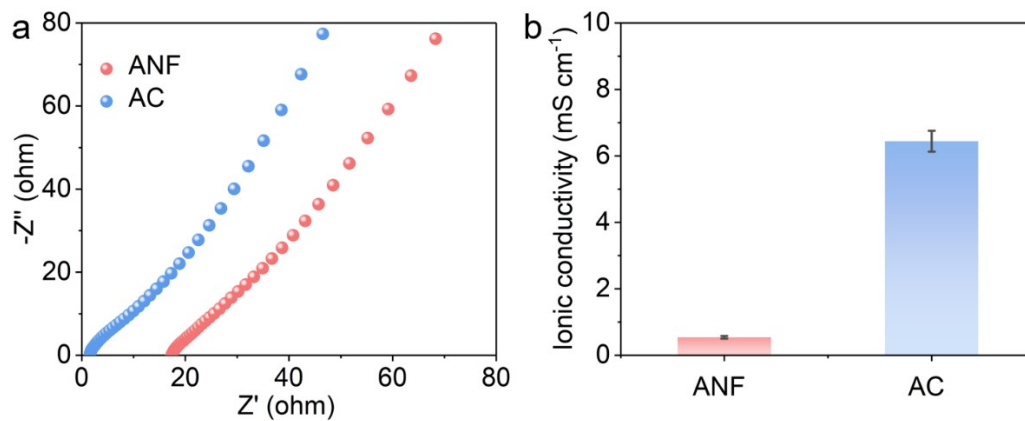


Figure S14. (a) Nyquist plots of stainless steel/membrane/stainless steel cells assembled with the ANF or AC membranes. (b) The ionic conductivity of the ANF and AC membranes.

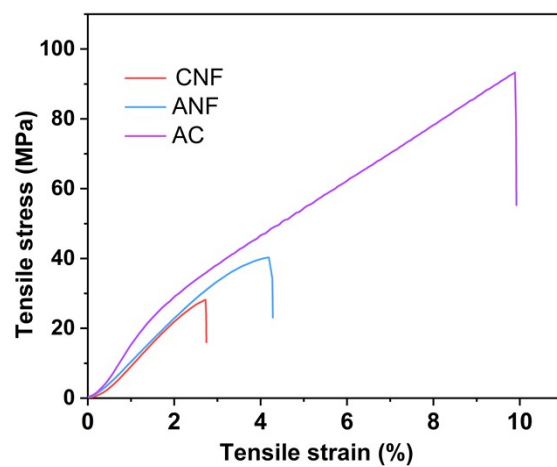


Figure S15. Tensile stress-strain curves of the electrolyte-wetted ANF, CNF, and AC membranes.

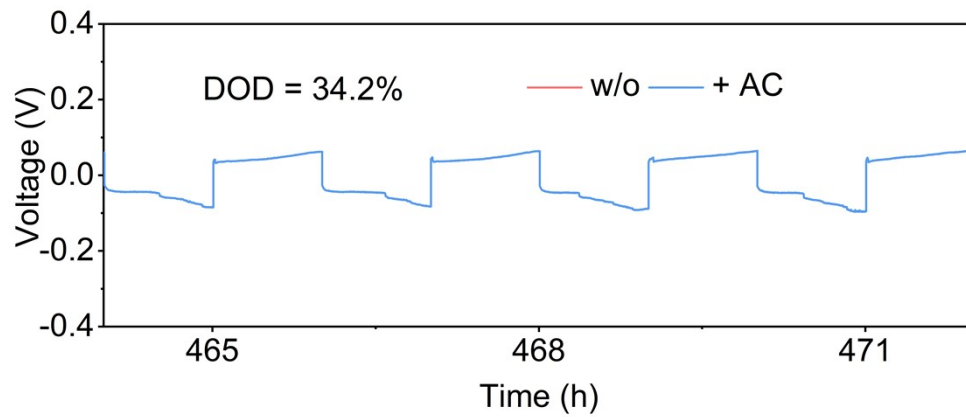


Figure S16. Voltage profiles of the Zn-symmetric cells with the AC interlayer and without an interlayer at a current density of 10 mA cm^{-2} with a cycling capacity of 10 mAh cm^{-2} .

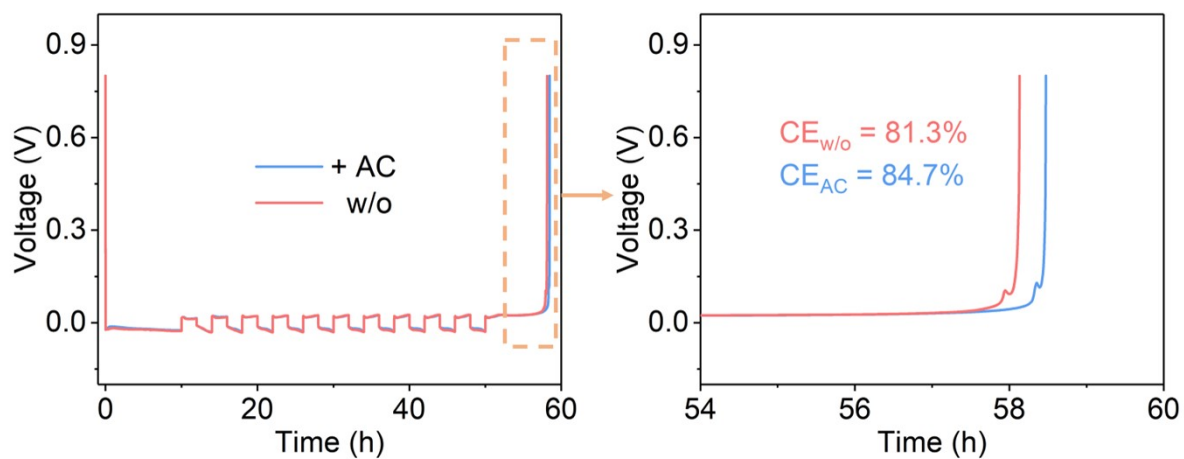


Figure S17. Voltage profiles of the asymmetrical Zn-Cu batteries with/without the AC interlayer.

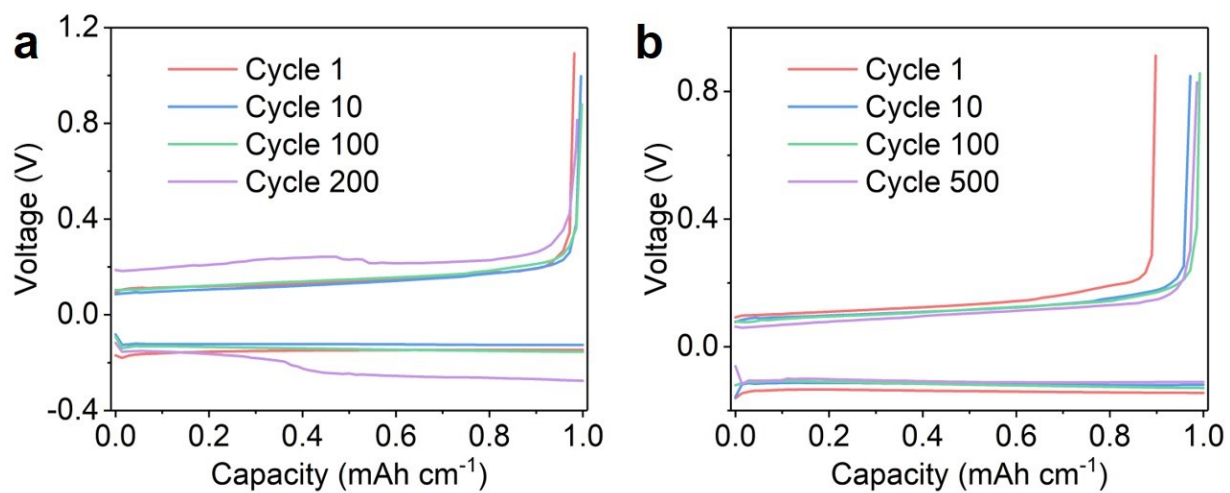


Figure S18. Voltage profiles of the asymmetrical Zn-Cu batteries (a) without and (b) with the AC interlayer at a cutoff potential of 0.8 V under 5 mA cm⁻² within 1 mAh cm⁻².

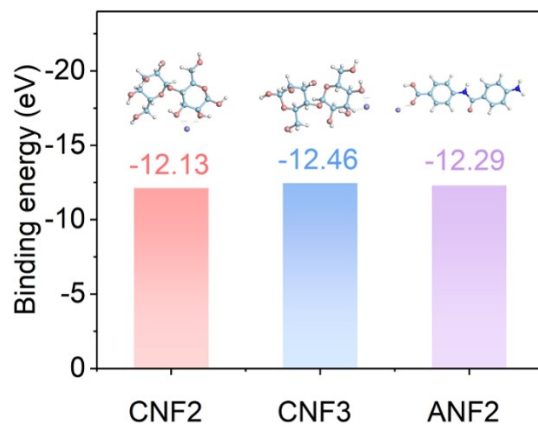


Figure S19. The DFT calculations for the binding energies of Zn²⁺ to CNF and ANF molecules.

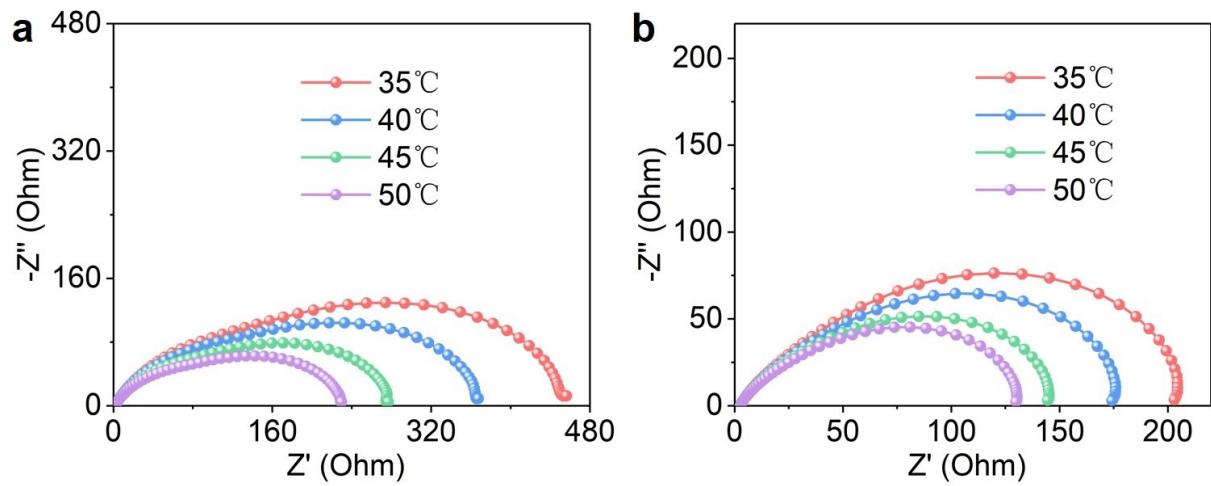


Figure S20. Nyquist plots of Zn symmetric cells (a) without and (b) with the AC interlayer under different temperatures.

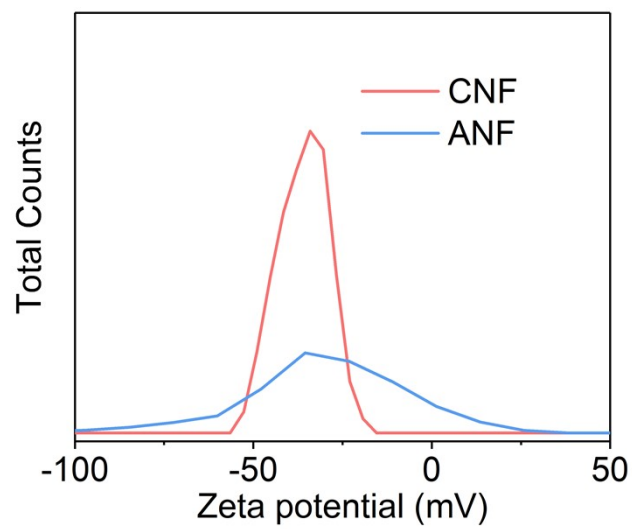


Figure S21. Zeta potential curve diagram of CNF and ANF.

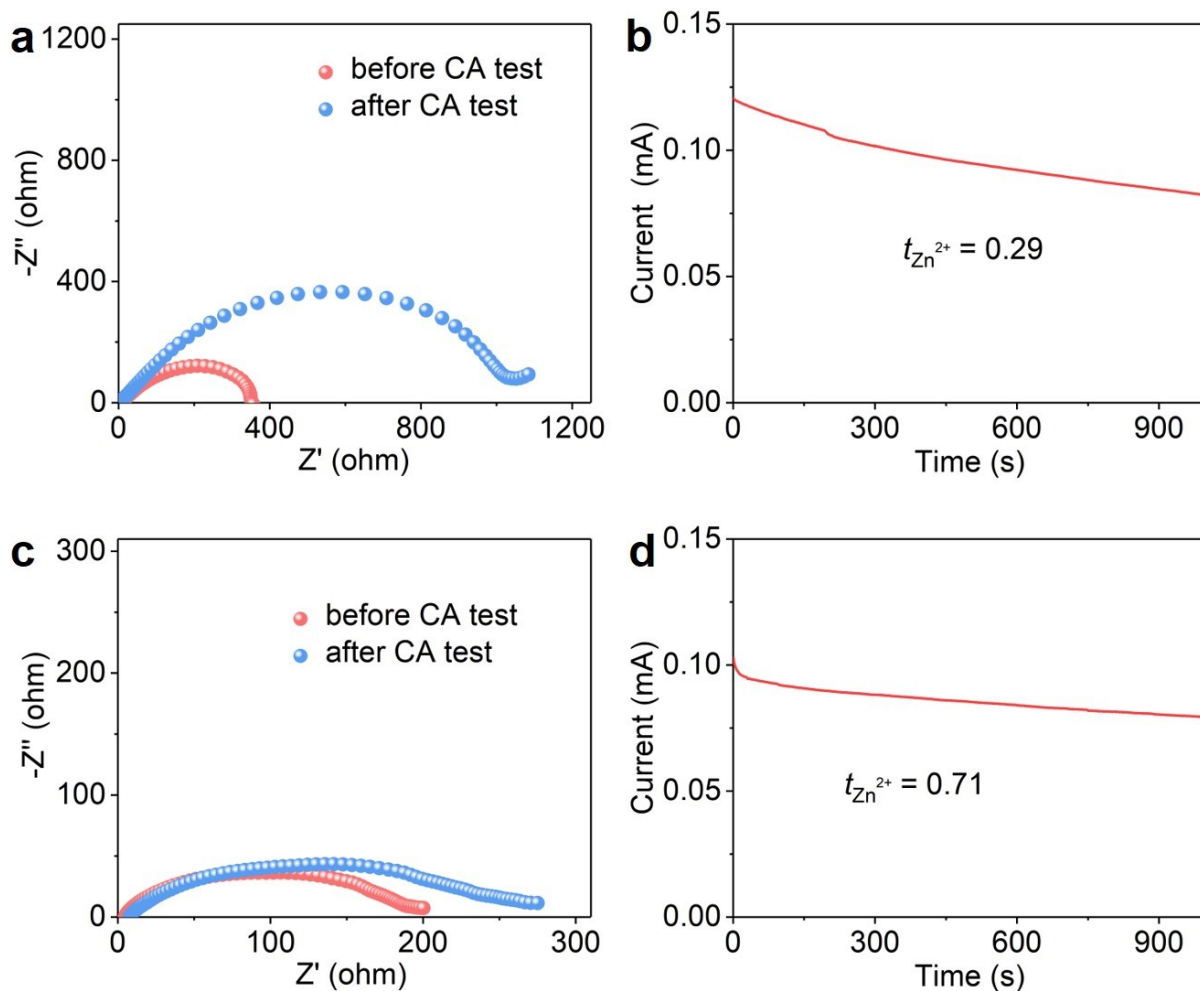


Figure S22. Nyquist plots of Zn symmetric cells before and after CA test (a) without and (c) with the AC interlayer. CA curves of Zn symmetric cells at a potential of 10 mV (b) without and (d) with the AC interlayer.

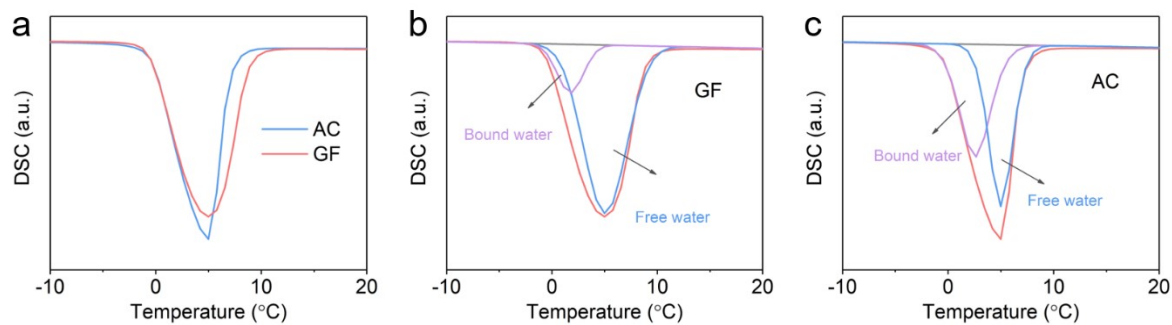


Figure S23 DSC curves of the AC and GF membranes wetted by water.

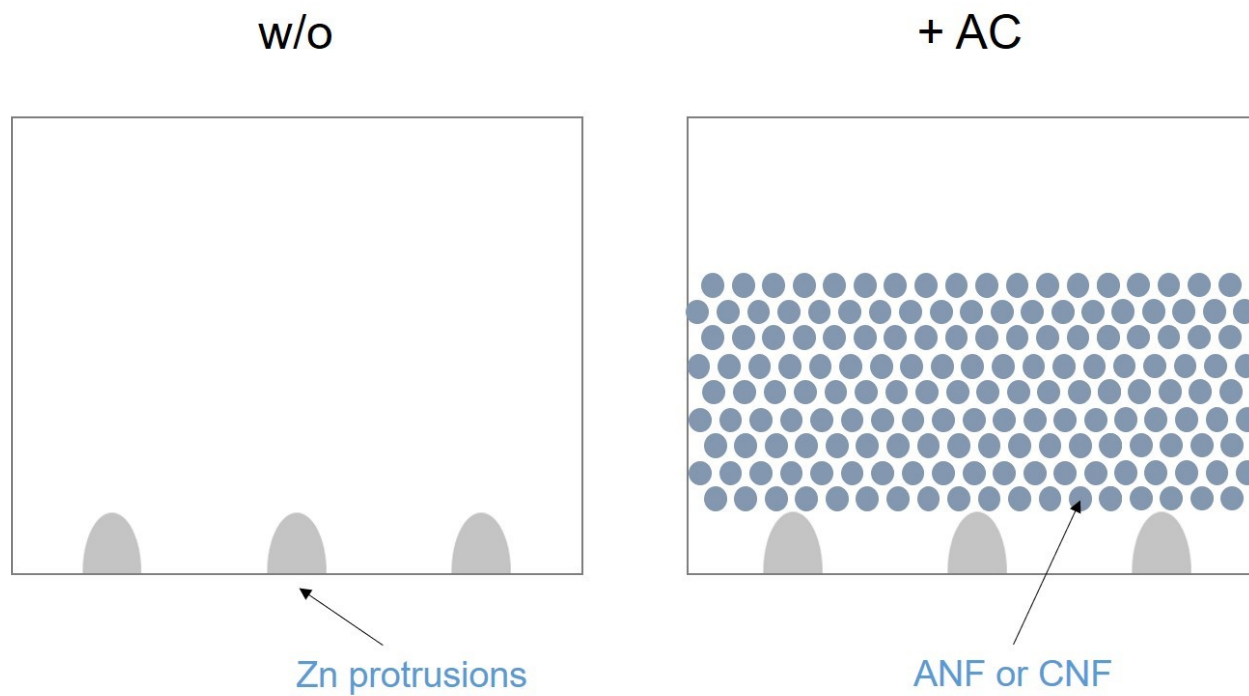


Figure S24. Original models involve the deposition of Zn^{2+} ions on the surface of Zn anodes.

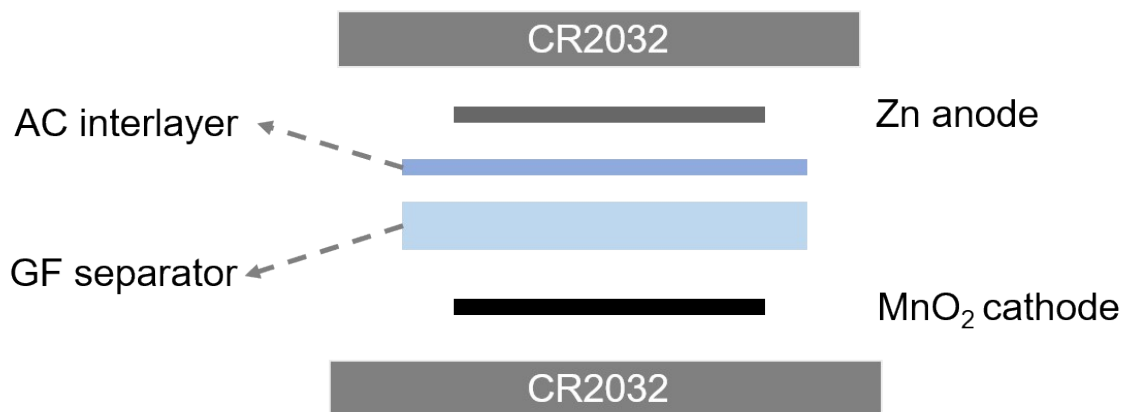


Figure S25. Schematic illustration for the assembly of the Zn-MnO₂ coin battery.

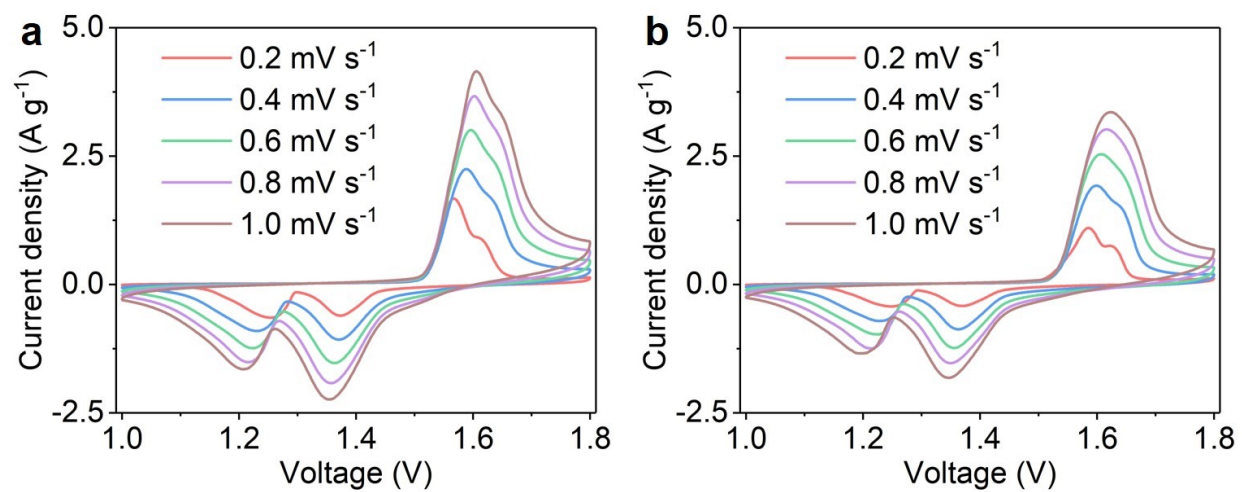


Figure S26. CV curves at various scan rates of Zn-MnO₂ batteries (a) with and (b) without the AC interlayer.

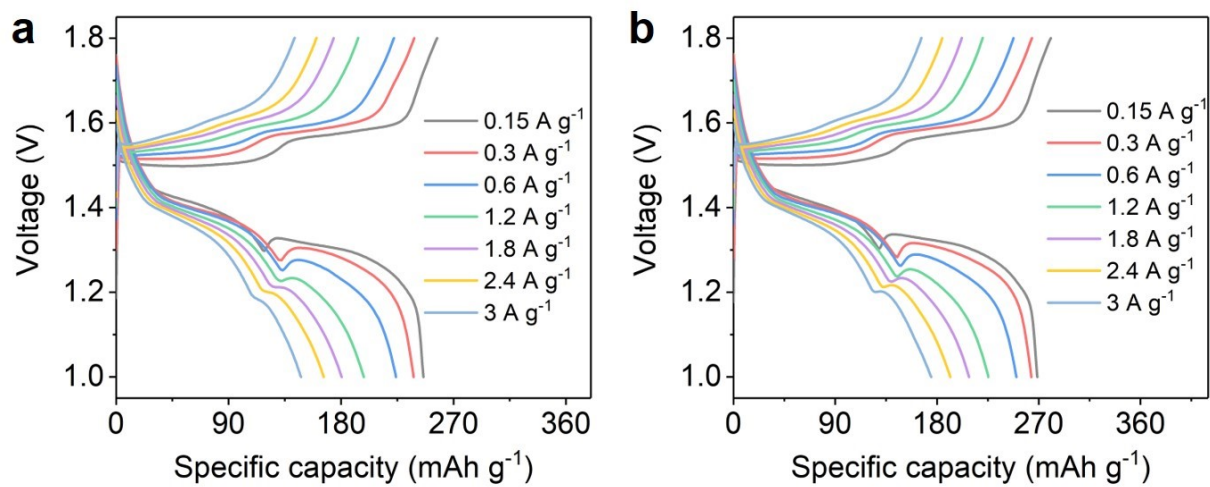


Figure S27. GCD curves at various current densities of Zn-MnO₂ batteries (a) without and (b) with the AC interlayer.

Tables

Table S1. The Mechanical properties of recently reported ANF-based membranes and the one in this study.

Membrane	Tensile Strength (MPa)	Fracture Energy (MJ m ⁻³)	Reference
ANF-MXene	201	22.3	29
ANF-RN	231	33	30
CNT-ANF	383	2.3	31
GO-PDA-ANF	437	23.9	32
AgNW-ANF	285.7	19.8	33
ANF-BNNS	167	6.16	34
ANF-MBLM	253.3	14.1	35
ANF	149.2	10.4	36
HAP-ANF	73.5	3.6	37
ANF-GO	181	30	38
ANF/CNF	303	39.9	This work

Table S2. Comparison of the lifespans of Zn anodes.

	Current density (mA cm ⁻²)	Cumulative capacity (mAh cm ⁻²)	Reference
WP+GF	1	1200	11
BPDA PE BisSF	5	1250	14
TCh	10	1600	15
FCNF	1	1000	28
DESM	0.1	500	42
UiO-66-GF	2	1650	43
MXene-GF	2	625	44
VG@GF	5	187.5	45
PAG@GF	8	2000	46
ANF/CNF	2	1776	This work
ANF/CNF	10	2375	This work

Video captions

Video S1. Demonstration of light-up bracelet powered by the pouch cell.

Video S2. Pouch cells continuously output when wearing the light-up bracelet on the wrist.